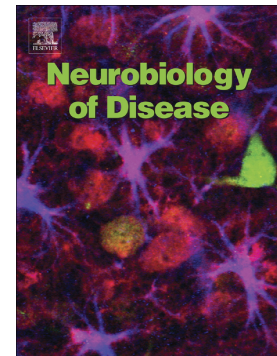


Wild-type p53-induced phosphatase 1 down-regulation promotes apoptosis by activating the DNA damage-response pathway in amyotrophic lateral sclerosis

Yue-Qing Yang, Yong-Hui Zheng, Chun-Ting Zhang, Wei-Wei Liang, Shu-Yu Wang, Xu-Dong Wang, Ying Wang, Tian-Hang Wang, Hong-Quan Jiang, Hong-Lin Feng



PII: S0969-9961(19)30323-7

DOI: <https://doi.org/10.1016/j.nbd.2019.104648>

Reference: YNBDI 104648

To appear in: *Neurobiology of Disease*

Received date: 22 March 2019

Revised date: 23 September 2019

Accepted date: 23 October 2019

Please cite this article as: Y.-Q. Yang, Y.-H. Zheng, C.-T. Zhang, et al., Wild-type p53-induced phosphatase 1 down-regulation promotes apoptosis by activating the DNA damage-response pathway in amyotrophic lateral sclerosis, *Neurobiology of Disease*(2018), <https://doi.org/10.1016/j.nbd.2019.104648>

This is a PDF file of an article that has undergone enhancements after acceptance, such as the addition of a cover page and metadata, and formatting for readability, but it is not yet the definitive version of record. This version will undergo additional copyediting, typesetting and review before it is published in its final form, but we are providing this version to give early visibility of the article. Please note that, during the production process, errors may be discovered which could affect the content, and all legal disclaimers that apply to the journal pertain.

Wild-type p53-induced Phosphatase 1 Down-regulation Promotes Apoptosis by Activating the DNA Damage-response Pathway in Amyotrophic Lateral Sclerosis

Yue-Qing Yang^a, Yong-Hui Zheng^a, Chun-Ting Zhang^a, Wei-Wei Liang^b, Shu-Yu Wang^a, Xu-Dong Wang^a, Ying Wang^a, Tian-Hang Wang^a, Hong-Quan Jiang^a, Hong-Lin Feng^{a,*}

^aDepartment of Neurology, The First Affiliated Hospital of Harbin Medical University, Harbin, Heilongjiang Province, PR China

^bDepartment of Neurology, The Second Affiliated Hospital of Harbin Medical University, Harbin, Heilongjiang Province, PR China

***Corresponding author:** Hong-Lin Feng

Department of Neurology

The First Affiliated Hospital of Harbin Medical University

Abbreviations: ALS, amyotrophic lateral sclerosis; ATM, ataxia-telangiectasia mutated; C9orf72, chromosome 9 open reading frame 72; CHK2, checkpoint kinase 2; HIPK2, homeodomain-interacting protein kinase 2; IR, ionizing radiation; pLV, puromycin lentivirus vector; SOD1, superoxide dismutase 1; Wip1, Wild-type p53-induced phosphatase 1

Harbin, Heilongjiang Province, PR China

Phone: +086-451-85555666

Fax: +086-451-53605867

Email: fenghonglin186@sina.com

Journal Pre-proof

Abstract

Accumulation of DNA damage has been detected in the spinal cord of patients as well as in the G93A mouse model of amyotrophic lateral sclerosis (ALS). Wild-type p53-induced phosphatase 1 (Wip1) is a p53-inducible serine/threonine phosphatase that terminates DNA-damage responses via dephosphorylation of DNA-damage response proteins, namely ataxia-telangiectasia mutated (ATM) kinase, checkpoint kinase 2, and p53, thus enhancing cell proliferation. However, the role of Wip1, DNA-damage responses, and their interaction in ALS development remains to be elucidated. Here, we showed that Wip1 expression levels were substantially decreased in ALS motor neurons compared with wild-type controls both *in vivo* and *in vitro*. The DNA-damage response was activated in superoxide dismutase 1 (SOD1)^{G93A}-transfected cells. However, increased expression of Wip1 improved cell viability and inhibited the DNA-damage response in mutated SOD1^{G93A} cells. Further studies demonstrated that decreased Wip1 expression reduced cell viability and further activated the DNA-damage response in chronic H₂O₂-treated NSC34 cells. In contrast, Wip1 promoted cell survival and suppressed DNA damage-induced apoptosis during persistent DNA damage conditions. Over-expression of Wip1 in the central nervous system (CNS) can delay the onset of disease symptoms, extended the survival, decreased MN loss improved motor function and inhibit the DNA-damage response in SOD1 G93A mice. Furthermore, homeodomain-interacting protein kinase 2 (HIPK2) promoted the degradation of Wip1 via the ubiquitin-proteasome system during chronic stress. These findings indicate that persistent accumulation of DNA damage and subsequent chronic activation of the downstream DNA damage-response ATM and p53 pro-apoptotic signaling pathways may trigger neuronal dysfunction and neuronal death in ALS.

Wip1 may play a protective role by targeting the DNA-damage response in ALS motor neurons. Importantly, these findings provide a novel direction for therapeutic options for patients with ALS.

Keywords: Wip1, HIPK2, DNA damage response, cell death, ALS

Introduction

Amyotrophic lateral sclerosis (ALS) is a chronic progressive fatal motor neuron disease characterized by selective loss of motor neurons (Boillée et al., 2006; Kiernan et al., 2011; Turner et al., 2011). Several genes, including chromosome 9 open reading frame 72 (*C9orf72*) repeat expansions (DeJesus-Hernandez et al., 2011), Cu-Zn superoxide dismutase (*SOD1*) (Rosen et al., 1993) and TAR DNA-binding protein (Sreedharan et al., 2008) have been shown to be implicated in ALS. Mutations in the *SOD1* gene are involved in 20% of familial ALS cases and in 5% of sporadic ALS cases (Majoor-Krakauer et al., 2003; Robberecht and Philips, 2013). Animal models based on *Sod1* mutations have revealed the key clinical manifestations of human disease, including motor neuron degeneration, muscle amyotrophy, and paralysis (Saccon et al., 2013; Turner and Talbot, 2008). In addition, the ALS-SOD1 animal model presents the complex pathology of the disease, including oxidative stress, mitochondrial dysfunction, DNA damage accumulation, and glutamate excitability toxicity (Rothstein, 2009). However, the exact mechanism and pathology of the initiation and development of motor neuron degeneration are still largely unknown.

Oxidative DNA damage measured as the content of 8-hydroxy-2'-deoxyguanosine is increased in hSOD1G93A transgenic mouse models (Aguirre et al., 2005; Amante et al., 2010) and patients with ALS (Blasco et al., 2017; Bogdanov et al., 2000; Ferrante et al., 1997; Mitsumoto et al., 2008; Murata et al., 2008; Shibata et al., 2000). In addition, DNA strand breaks may significantly contribute to the pathology of ALS (Madabhushi et al., 2014; Martin, 2007; Martin et al., 2007). The DNA damage response is an elaborate signaling process that involves the location of DNA lesions, transduction of the signal, and instruction of cellular enzymes to repair the damaged

DNA. Ataxia-telangiectasia mutated (ATM) protein is a phosphatidylinositol 3-kinase (PI3K)-like kinase that is selectively activated by double-stranded DNA breaks (Ditch and Paull, 2012; McKinnon, 2004; Shiloh and Ziv, 2013). ATM mediates cellular responses to DNA damage by phosphorylating its many downstream proteins, including checkpoint kinase 2 (CHK2), thus promoting cell cycle arrest to facilitate DNA damage repair. Another key function of ATM is to activate apoptosis by directly phosphorylating p53 when DNA damage is too extensive (Ciccia and Elledge, 2010). ATM and p53 are increased in the spinal cord of patients with ALS caused by *C9orf72* repeat expansions (Farg et al., 2017). However, the precise mechanisms linking the DNA damage response to ALS remain poorly understood.

Wild-type p53-induced phosphatase 1 (Wip1), a member of the serine/threonine phosphatase PP2C family, inhibits stress signaling and promotes the return of a cell to homeostasis once the damage has been repaired. The expression of Wip1 is induced by multiple stresses, such as ionizing radiation (IR), ultraviolet radiation, and hydrogen peroxide (H₂O₂) (Chew et al., 2009; Fiscella et al., 1997; Lowe, et al., 2010; Takekawa et al., 2000). Wip1 directly dephosphorylates several key signaling proteins involved in stress signaling, including ATM, CHK2, p53, p38 MAPK, MDM2, and the p65 component of the NF- κ B complex, all of which play critical roles in apoptosis, the cell cycle, and DNA repair (Macurek et al., 2010; Shreeram et al., 2006a; Shreeram et al., 2006b). Wip1 not only plays a protective role in DNA damage-induced apoptosis, but also in other types of oxidative stress, such as manganese-induced neuron apoptosis (Ma et al., 2015; Shreeram et al., 2006b; Xia et al., 2009).

Here, the aim of the present study was to determine whether Wip1, a critical player in the DNA damage response, affects the survival of motor neurons in ALS. We found that Wip1 was down-regulated in a mouse model of ALS and mSOD1 NSC-34 cells. Our work suggests that down-

regulation of Wip1 is required for chronic activation of the ATM signaling pathway. And homeodomain-interacting protein kinase 2 (HIPK2) promoted Wip1 degradation through the ubiquitination system in hSOD1^{G93A} cells. We propose a neurotoxic effect of HIPK2-Wip1-ATM dysregulated mechanism during persistent and irreversible DNA damage in ALS. These findings suggest novel therapeutic targets for ALS.

Material and Methods

Experimental animals

Transgenic mice with a mutant SOD1 G93A gene (B6SJL-Tg (SOD1-G93A) 1Gur/J) overexpression (Gurney et al., 1994) were purchased from Jackson Laboratory (Stock no. 002726; BarHarbor,ME,USA). A colony of SOD1 G93A mice was maintained by breeding SOD1 G93A mice with non-transgenic C57/BL6 mice. Animals were group-housed under standard housing conditions with a 12 h light-dark cycle, and food and water ad libitum. Mouse DNA was extracted to determine the genotypes of transgenic mice by polymerase chain reaction (PCR) as described previously (Maier et al., 2013). Non-transgenic littermates not expressing the SOD1 G93A were used as wild-type controls. Mouse studies were conducted according to a protocol approved by the Harbin Medical University Experimental Animal Research Ethics Committee. Every effort was made to minimize the number of animals used and their suffering.

Cell culture

The mouse motor neuronal cell line NSC34 (a gift from Dr. Neil Cashman, University of British Columbia, Canada) is a hybrid of the embryonic mouse spinal cord motor neuron and the neuroblastoma cell line (Maier et al., 2013); These cells exhibit many motor neuron characteristics including extension of neuritis, generation of action potentials, expression of

neurofilament proteins and choline acetyltransferase, synthesis and storage of acetylcholine, and induction of twitching in co-cultured muscle cells (Maier et al., 2013). The cells were maintained in Dulbecco's modified Eagle's medium (DMEM) supplemented with 10% (v/v) fetal bovine serum (FBS) and 100 units of penicillin-streptomycin and cultured at 37°C in a 5% CO₂ incubator.

Production of a stable hSOD1^{G93A}-transfected NSC34 cell line

NSC34 cells were cultured and stably transfected with mutant human G93A SOD1 (mSOD1 cells). The control cells were transfected with wild-type human SOD1 (wtSOD1 cells) or empty puromycin lentivirus vector (pLV cells) as described previously (Yin et al., 2015). Stable cell clones were maintained in 200 µg/ml of puromycin (G418, Invitrogen, Paisley, UK).

Primary neuronal culture

For primary neuronal culture, the brain was removed from E17–19 embryos, and after trypsinization, the cells were filtered through a 220-mesh filter to remove the tissue debris. Cells were centrifuged, re-suspended, and seeded in complete neurobasal medium with 2% B-27, 0.5 mM glutamine (Invitrogen), and penicillin-streptomycin and cultured at 37°C in a humidified incubator under 5% CO₂. Half of the culture medium was changed every second day.

Small-interfering RNA

RNA interference experiments were performed according to the manufacturer's instructions. The siRNA-specific sequences of mouse Wip1 were designed and synthesized at Shanghai GenePharma Co., Ltd. (Shanghai, China) and siRNA-specific sequences of mouse HIPK2 were

purchased from Santa Cruz Biotechnology (Santa Cruz, CA, USA). The siRNAs were transiently transfected in mSOD1 cells using Lipofectamine 2000 reagent (Invitrogen Life Technologies). At 48 h post-transfection, the cells were rinsed and RNA/protein was collected. The following Wip1 siRNA (si-Wip1) sequences were used: 5'-GGA AUU CAG GAU GAC CCA ATT-3' and 5'-UUG GGU CAU CCU GAA UUC CTT -3'. The following sequences were used for the negative control (si-NC): 5'-UUC UCC GAA CGU GUC ACG UTT-3' and 5'-ACG UGA CAC GUU CGG AGA ATT-3'.

Plasmids and transient transfections

Flag-tagged mouse Wip1 expression vector and mouse HA-tagged HIPK2 expression vector were purchased from GeneCopoeia, Inc. (Guangzhou, China). The p3xFlag-CMV-14 construct (Sigma-Aldrich, St. Louis, MI, USA) was used as a control. The plasmids were transiently transfected using Lipofectamine2000 reagent (Invitrogen Life Technologies). Briefly, mSOD1 cells or NSC34 cells were seeded at a density of 1×10^6 cells per well onto 6-well plates 24 h prior to transfection. For the overexpression of Wip1 in mSOD1 cells, the Flag-Wip1 plasmid (2 μ g per well) was diluted in 200 μ l Opti-MEM (Invitrogen Life Technologies) in a separate tube, and Lipofectamine2000 (4 μ l per well) was diluted in 200 μ l Opti-MEM in a different tube. Following incubation for 5 min, Lipofectamine2000 was added to the DNA solution for Lipofectamine2000/DNA-complex formation. After incubation for 20 min, the mixture was added drop-wise to the cell culture plate. The cells were incubated in 5% CO₂ for 6 h. After transfection, the cell culture medium was replaced with fresh DMEM that contained 10% FBS and subsequently cultured for 48 h for subsequent experiments.

Immunohistochemistry and immunofluorescent staining

Spinal cords of three SOD1 G93A mice and three its non-transgenic littermates were fixed, paraffin-embedded, and sliced as described previously (Feng et al., 2008; Wang et al., 2015; Yin et al., 2015). Briefly, 6- μ m sections were cut and one section from every fourth section were analyzed to avoid capturing the same cell in different sections. Sections were incubated with a primary antibody against mouse monoclonal Wip1 antibody (1:100;sc-376257;Santa Cruz) overnight at 4°C. Then sections were incubated with secondary antibodies (Abcam, Cambridge, MA, USA) for 2 h at room temperature. The staining was visualized using 3,3'-diaminobenzidine (DAB). Images of the specimens were captured using a Zeiss Axiophot microscope (Carl Zeiss AG, Jena, Germany). At least six separate sections per animal were analyzed. Semiquantitative expression of Wip1 was calculated using Image-Pro Plus 6.0 software by an experienced pathologist who was blinded to the sample groups. For quantification of ChAT-positive cells of lumbar spinal cord sections. Three mice of each group were euthanized at 130 days of age, when motor deficits were apparent. The mice were anesthetized and transcardially perfused with phosphate-buffered saline (PBS) for 10 min, followed by 4% paraformaldehyde in 0.1% phosphate buffer (PB) for 30 min. The spinal cord was dissected and post-fixed with 4% paraformaldehyde. The lumbar spinal cord was paraffin-embedded and sectioned at a thickness of 6- μ m. To quantify the number of motor neurons, every 4th section was selected, with a total of 30 sections being collected for each animal. The spinal cord sections were immunostained with choline acetyltransferase (ChAT), a specific marker of MNs in the anterior horn (Abcam, ab178850, 1:2000). (ChAT), then sections were incubated with secondary antibodies (Abcam, Cambridge, MA, USA) for 2 h at room temperature. The staining was visualized using 3,3'-diaminobenzidine (DAB). Images of neurons were captured under a Leica microscope (Leica,

Wetzlar, Germany). The number of motor neurons (6 sections per mouse) was determined by an experienced pathologist who was blinded to the sample groups.

For immunofluorescence staining, the spinal cord sections (6 sections per mouse) of three SOD1 G93A mice and three its non-transgenic littermates were incubated with primary antibodies overnight at 4°C. The following antibodies were used: mouse monoclonal Wip1 antibody (1:100; sc-376257; Santa Cruz); rabbit anti- γ H2AX (pSer139) (1:100, 9718, Cell Signaling Technology) and rabbit anti- Cleaved Caspase-3 (Asp175) (1:100, 9661, Cell Signaling Technology) and rabbit (bs-1369R) or mouse (bsm-33073M) anti-MAP-2 (1:200, microtubule-associated protein-2, Beijing Bioss Biotechnology Co., Beijing, China). Secondary antibodies conjugated with Alexa Fluor 488 or 594 (ZSGB-BIO, Beijing, China) were subsequently applied. The images were observed using a fluorescence microscope (Olympus, Tokyo, Japan) by an experienced pathologist who was blinded to the sample groups. At least four separate fields were analyzed.

Immunofluorescence cytochemistry analysis

The cells were sequentially fixed with 4% paraformaldehyde, permeabilized in 0.1% Triton X-100 (Sigma), blocked with 5% bovine serum albumin (BSA), and then incubated with anti-Wip1 (1:100; sc-376257; Santa Cruz) overnight at 4°C. Antibody binding was visualized using Alexa Fluor 488-label goat anti-rabbit IgG (1:100, ZSGB-BIO). DAPI (Sigma) (5 μ g/ml for 3 min) was used for nuclei counterstaining. Images were obtained using a fluorescence microscope (Olympus) by an experienced pathologist (Harbin Medical University, China) who was blinded to the identity of each group. Each experiment was performed in duplicate with three independent samples. Each sample was run in triplicate wells.

Quantitative real-time PCR (qRT-PCR)

Total RNA was extracted from cells and spinal cord tissues using TRIzol reagent (Invitrogen Life Technologies). qRT-PCR for mouse Wip1 and endogenous mouse β -actin was performed on a Light Cycler 480 (Roche, Basel, Switzerland) using the One-Step SYBR PrimeScript RT-PCR Kit II (Takara Biotechnology Co., Dalian, China) according to the manufacturer's instructions. The following primer sequences were used: Wip1: 5'-CAATTGGCCTTGTGCCTACT-3' (forward), 5'-TCTTTCGCT GTGAGGTTG TG-3' (reverse); and β -actin: 5'-CCAGCCTTCCTTGGGTAT-3' (forward), 5'-TGCTGCTGGAAGGTGGACAGTGAG-3' (reverse). The relative mRNA transcription was expressed as a percentage of the control conditions using the $2^{-\Delta\Delta C_t}$ method, where C_t is the threshold cycle value. Each experiment was performed in duplicate with five independent samples. Each sample was run in triplicate wells.

Immunoblotting and immunoprecipitation

The cells and spinal cord tissues were lysed in RIPA buffer (Beyotime Institute of Biotechnology, Jiangsu, China) containing protease inhibitor (10 μ g/ml PMSF) for 30 min on ice. To detect phosphorylated protein, a phosphate and protease inhibitor cocktail (04693132001, Roche Diagnostics) was also applied to inhibit dephosphorylation. The protein concentration was determined using the BCA Protein Assay Kit (Beyotime Institute of Biotechnology). The proteins were subjected to sodium dodecyl sulfate polyacrylamide gel electrophoresis (SDS-PAGE) and then transferred to polyvinylidene fluoride membranes using a semi-dry electrophoretic transfer cell (Bio-Rad, Hercules, CA, USA). The blots were blocked for 2 h in tris-buffered saline and Tween 20 containing 5% non-fat dry milk or 5% BSA at room

temperature. The blots were probed with primary antibodies overnight at 4°C. The following antibodies were used: mouse anti-Wip1 antibody (1:800; sc-376257, Santa Cruz), mouse anti-Flag (1:5000, F1804, Sigma), rabbit anti-ATM (1:1000, EPR17059, Abcam), rabbit anti-p-ATM (Ser1981) (1:1000, EP1890Y, Abcam), rabbit anti-p-Chk2 (Thr68) (1:1000, ab85743, Abcam), rabbit anti-Chk2 (1:1000, 2662, Cell Signaling Technology), rabbit anti-p-p53 (Ser15) (1:1000, 9284, Cell Signaling Technology), and mouse anti- β -actin (1:1000, ZSGB-BIO). Secondary IRDye800-conjugated goat anti-mouse IgG or goat anti-rabbit IgG (1:10000, Li-COR) were used at 37°C for 1 h. The blots were visualized using the Odyssey infrared imaging system (Li-COR Biotechnology, Lincoln, NE, USA) and quantified using ImageJ (National Institutes of Health, Bethesda, MD). The blots were quantified and normalized with β -actin as an internal loading control.

For immunoprecipitation, the cells were suspended in NP-40 lysis buffer containing protease inhibitors, and the lysates were centrifuged at 12,000 rpm for 10 min. Bradford assays were performed to ensure equal protein loading. Equal amounts of protein were precipitated with Flag antibody (F1804, Sigma) or HIPK2 antibody (EPR3819, Abcam) overnight at 4°C on a rocker. The following day, protein A/G agarose beads (Santa Cruz) were added to each sample and incubated for 4 h at 4°C. Immunoprecipitates were collected by centrifugation and then washed five times with NP-40 lysis buffer at 4°C. The agarose beads were re-suspended in 40 μ l of 1 \times SDS-PAGE sample buffer and incubated at 100°C for 10 min. Following a pulse spin, whole cell lysates and immunoprecipitates were separated by SDS-PAGE and transferred onto polyvinylidene difluoride membranes. Membranes were immunoblotted with indicated antibodies.

Cell apoptosis and cell viability assessments

NSC34 cells were seeded in a 6-well plate and transfected with Wip1 expression vector or siRNA for 48 h after treatment for different times with 100 μ M H₂O₂ (3, 6, 24, or 48 h) or control (0.9% normal saline) at 37°C. For the apoptosis assay, the cells were stained with FITC Annexin V and PI (BD, San Jose, CA, USA) according to the manufacturer's instructions to detect apoptotic cells. The tests were repeated in quadruplicate. Cell viability was determined using CCK-8 assay in accordance with the manufacturer's instructions. Briefly, NSC34 cells were seeded at a density of 2×10^4 cells/well in 100 ml DMEM complete medium in a 96-well plate and transfected with Wip1 expression vector or siRNA for 48 h after treatment for different times with 100 μ M H₂O₂ (3, 6, 24, or 48 h) or control (0.9% normal saline) at 37°C. Thereafter, the medium of the cells was removed and replaced with 90 ml DMEM complete medium plus 10 ml CCK-8 solution. The cells were then incubated at 37°C for an additional 2 h. Cell viability was determined by measuring the optical density (OD) of the dissolved formazan product at 490 nm by a microplate reader (ELx808, Bio-Tek Instruments, Milan, Italy) with a reference wavelength of 630 nm. The assays were performed using triplicate independent cell cultures.

Lentivirus preparation and Intracerebroventricular (i.c.v) injection

The lentivirus(10^9 TU/ml) for overexpressing Wip1 (LV-Wip1) and the control lentivirus (LV-GFP) were obtained commercially from GenePharma Corporation (Shanghai, China). Three predesigned small interfering RNA (siRNA) sequences targeting the Wip1 (GenBank accession number NM_016910) were designed by GenePharma Co., Ltd. (Shanghai, China) The specificity for Wip1 disruption was determined by transfecting the siRNAs into NSC34 cell lines according to the manufacturer's instructions (Invitrogen, Carlsbad, CA, USA). After screening to validated

potential siRNAs, the Wip1 target sequence (5'-GGA AUU CAG GAU GAC CCA ATT-3' and 5'-UUG GGU CAU CCU GAA UUC CTT-3') was selected for the construction with a lentiviral vector. A non-silencing sequence (5'-UUC UCC GAA CGU GUC ACG UTT-3' and 5'-ACG UGA CAC GUU CGG AGA ATT-3') was used as a negative control. At 90 d of age, 30 female ALS mice were randomly divided into groups as follow: LV-Wip1 treatment, LV-GFP treatment groups (n=15/group). At 90 d of age, 30 female ALS mice were randomly divided into groups as follow: LV-siRNA-Wip1 and LV-siRNA-NC groups (negative control group) (n=15/group). For intracerebroventricular injection, the mice were placed in a small animal stereotaxic frame (David Kopf Instruments, Tujunga, CA, USA). The skull was exposed and a small-hole craniotomy performed based on predetermined stereotaxic coordinates (lateral 1.6 mm and antero-posterior 1 mm to the bregma, and horizontal 2 mm from the dura mater) (Burton MD et al., 2011). 7 μ L of a mixture of lentiviral particles (10^9 TU/ml) containing Wip1 overexpression, Wip1 siRNA, or nontargeting control sequences were mixed with the cationic lipid polybrene (4 μ g/ μ L, GenePharma), incubated at 37°C for 15 min, and manually injected into the right cerebral lateral ventricle slowly for ≥ 20 min using a glass micro-needle (Drummond Scientific Company, PA)

Behavioral assessment and analysis

The time at which the mice could not stay on the rotating rod for 180 s was labeled as disease onset. (Li M et al., 2007). The disease endpoint was marked as the mouse being unable to right itself within 30 s after being placed on its side (both sides tested) (Ludolph et al., 2007). Rotarod performance was evaluated by measuring the retention time on a rotating rod (Harbin Lock Factory, Harbin, China) every four days. Specifically, motor performance in the rotarod test (16 rpm) was measured for each mouse starting at 70 days of age and after 1 week of training. Three

trials were performed for each animal, and the longest time spent on the rod (180 s max) was recorded as the retention time (Ludolph et al., 2007).

Statistical analysis

Statistical analyses were performed using GraphPad Prism software (www.graphpad.com; version 5.01 for Windows, San Diego, CA, USA). Data are presented as the mean \pm standard error of the mean (SEM). Differences between the two groups were compared using a Student's *t* test. Differences between multiple groups were evaluated using one-way analysis of variance, followed by Dunnett's post hoc test. The log-rank test was performed to analyze survival and disease onset times. $P < 0.05$ was considered statistically significant.

Results

Wip1 expression

In the first series of experiments, we determined whether the level of Wip1 differed between hSOD1^{G93A}-negative and hSOD1^{G93A}-positive mice using immunohistochemistry. Immunohistochemical staining of Wip1 was observed in the slices of the 130-day-old SOD1^{G93A}-positive and SOD1^{G93A}-negative mice. Wip1 was mainly expressed in the cytoplasm of the dorsal horn of the spinal cord, and the immunoreactivity of the positive mice was decreased compared with that of the hSOD1G93A-negative mice (Fig. 1A), the OD values of Wip1 in the cervical spinal motor neurons and lumbar neurons of hSOD1^{G93A}-positive mice were lower than those of hSOD1G93A-negative mice ($p < 0.01$) (Fig. 1B). We also carried out spinal immunofluorescence double staining in hSOD1^{G93A}-positive mice and hSOD1^{G93A}-negative mice to confirm the results of immunohistochemistry (Fig. 2). Compared to hSOD1^{G93A}-negative mice, the number of motor neurons (red) in hSOD1^{G93A}-positive mice was significantly reduced.

The expression of Wip1 (green) in the motor neurons of hSOD1^{G93A}-positive mice was weaker than that in the motor neurons of hSOD1^{G93A}-negative mice. Western blot analysis was conducted to semi-quantitate the protein levels of Wip1 in the spinal cords of the two groups. Compared with the hSOD1^{G93A}-negative mice, the hSOD1^{G93A}-positive mice exhibited significantly reduced Wip1 protein levels ($p<0.05$) (Fig. 1C and D). qRT-PCR was subsequently performed to assess Wip1 mRNA expression. The Wip1 mRNA levels were substantially decreased in the spinal cord of the hSOD1^{G93A}-positive mice than that of the hSOD1^{G93A}-negative mice ($p<0.05$) (Fig. 1E).

In previous studies, the expression of Wip1 was increased after the cells were subjected to transient DNA damage induced by transient IR (Song et al., 2013). To investigate the change in Wip1 expression in primary neurons from mSOD1-positive mice, we confirmed that the fluorescence intensity of Wip1 in the nucleus of mSOD1-positive primary neurons was significantly stronger than that of SOD1-negative primary neurons (Fig. 3A). qRT-PCR analysis indicated that the mRNA level of Wip1 in mSOD1-positive primary neurons was significantly higher than in mSOD1-negative primary neurons ($p<0.01$) (Fig. 3B). NSC34 cells stably transfected with pLV (empty vector), wtSOD1, or mutant human SOD1G93A (mSOD1) were used as *in vitro* ALS models. Western blot analysis showed a decrease in Wip1 protein levels in mSOD1 cells ($p<0.05$) (Fig. 3C and D) compared to NSC34, pLV, and wtSOD1 cells. The qRT-PCR results showed a reduction in mRNA levels of Wip1 in mSOD1 cells compared to control cells ($p<0.05$) (Fig. 3E).

DNA damage is reportedly increased in the ALS mouse model and ALS patients (Blasco et al., 2017; Bogdanov et al., 2000; Ferrante et al., 1997; Mitsumoto et al., 2008; Murata et al., 2008; Shibata et al., 2000). In the present study, we showed an increase in γ -H2AX reactivity (DNA

damage marker, Fig. 4) and cleaved caspase3 immunofluorescent staining (a hallmark of apoptosis, Fig. 5) in hSOD1G93A-positive mice.

In summary, the expression levels of Wip1 were substantially reduced in the spinal cord motor neurons of ALS transgenic (G93A) mice. Consistent with the *in vivo* data, the levels of Wip1 were decreased *in vitro* in mSOD1 cells. However, the protein and mRNA levels of Wip1 were increased in primary neurons from ALS transgenic mice, which is opposite to the Wip1 expression level in end-stage hSOD1^{G93A}-positive mice.

Decrease in Wip1 protein level during chronic stress conditions

Wip1 functions as a homeostatic regulator of the ATM-mediated DNA damage response-signaling pathway upon exposure to IR (Shreeram et al., 2006a), and chronic activation of the DNA damage response is associated with cell death in neurodegenerative diseases (Gao et al., 2015; Lu et al., 2014). Therefore, we investigated whether Wip1 modulates cell viability and DNA damage response signaling during H₂O₂-induced neuron apoptosis. We treated the primary cultured neurons and NSC34 motor neuron-like cells with 100 μ M H₂O₂ for the indicated time (Doré et al., 1999; Lee et al., 2016b; Singhal et al., 2013). Western blot analysis showed that the expression of Wip1 in NSC34 cells was significantly increased at 6 h after H₂O₂ treatment, followed by a gradual decrease starting from 24 h after treatment (Fig. 6A). We tested whether Wip1 activation was involved in inhibiting apoptosis and suppressing activation of DNA damage response signaling. As shown in Fig. 6A, 6 h after H₂O₂ treatment (***p < 0.001), Wip1 activation correlated inversely with the ATM, CHK2, and p53 phosphorylation state. Increase of cleaved caspase 3, a hallmark of cell apoptosis, activation of the DNA damage response signaling, and down-regulation of Wip1 were observed concurrently after 24 h of H₂O₂ treatment (*p < 0.05, **p < 0.01, ***p < 0.001) (Fig. 6A and 6B). Expression of Wip1 in the primary

cultured neurons was robustly increased at 1 h after H₂O₂ treatment, decreased at approximately 6 h, and was very diminished at 12 h (Fig. 6C).

Wip1-mediated dephosphorylation of DNA damage response signaling delays apoptotic death in neurons

To confirm the direct association between Wip1 activation and apoptosis during H₂O₂-induced oxidative damage, we knocked out Wip1 in NSC34 cells using si-RNA. Wip1 silencing increased phosphorylation of ATM, CHK2, and p53 (*p < 0.05, **p < 0.01, ***p < 0.001) (Fig. 7A and B). It is important to note that the silencing of Wip1 caused significant apoptosis after H₂O₂ treatment; as seen in NSC34 cells, the intensity of the immunoreactivity of cleaved caspase-3 was stronger after Wip1 depletion (*p < 0.05, ***p < 0.001) (Fig. 7A and B). In the absence of Wip1, more than 30% of the cells died during the 6 h of H₂O₂ treatment, while the control cells remained resistant in the presence of Wip1(*p < 0.05, **p < 0.01) (Fig. 7C, D, and E). Flag-Wip1 overexpression in NSC34 cells delayed the activation of DNA damage response signaling (*p < 0.05, **p < 0.01, ***p < 0.001) (Fig. 8A and B) and inhibited H₂O₂-induced apoptosis (*p < 0.05, **p < 0.01) (Fig. 8C, D, and E). These data led us to consider that Wip1 activation after H₂O₂ treatment can stabilize DNA damage response signaling and inhibit cell death.

Overexpression of Wip1 improves cell viability and inhibits the DNA damage response in mSOD1 cells

To determine whether Wip1 had a cytoprotective effect against SOD1-induced toxicity, we used pLV (empty vector), wtSOD1, or mSOD1 lentivirus to transfect NSC34 cells stably. The expression of pATM, pCHK2, and p-p53 in mSOD1-expressing NSC34 cells was significantly increased compared to control cells (***p < 0.001) (Fig. 9A and B). mSOD1 and WTSOD1 cells

were transfected with Flag-Wip1 overexpression plasmids. After 48 h of transfection, we observed that ectopic expression of Wip1 significantly attenuated pATM, pCHK2, and p-p53 expression in both cases (* $p < 0.05$) (Fig. 9C and D). These changes were accompanied by improved mSOD1 NSC34 cell viability (### $p < 0.001$) (Fig. 9E). Although Wip1 also inhibited the levels of pATM, pCHK2, and p-p53 in wtSOD1 cells, the changes did not affect cell viability ($p > 0.05$) (Fig. 9E). These results showed that activation of the ATM/CHK2/p53 pathway reduced the viability of mSOD1 NSC34 cells, and the overexpression of Wip1 attenuated the activation of DNA damage response signal transduction induced by mSOD^{G93A}, ultimately improving SOD1 cell viability.

HIPK2 promotes Wip1 degradation through the ubiquitin-proteasome system in mSOD1 cells

Wip1 protein is maintained at a low level in cells under normal conditions, and expression is induced by p53 after g-irradiation (Fiscella et al., 1997). Wip1 can be regulated at the protein level as well as the transcriptional level as a fast and efficient way to maximize quick responses to DNA-damage stress (Chew et al., 2009; Choi et al., 2013; Fiscella et al., 1997; Lowe et al., 2010; Takekawa et al., 2000). In the previous studies, the mRNA of Wip1 was decreased in *in vitro* and *in vivo* models of SOD1^{G93A} (Fig. 1E and Fig. 3E). However, the level of p53, a transcription factor of Wip1, was increased in mSOD1 cells (Fig. 6A). Another transcription factor, CREB, which can regulate the transcription of Wip1 both basally and after DNA damage independent of p53 (Rossi et al., 2008), was decreased in mSOD1 cells (Yin et al., 2015). Other than at the transcriptional level, Wip1 can also be regulated at the protein level through the ubiquitin-proteasome system. HIPK2 is a protein kinase that targets Wip1 for phosphorylation and proteasomal degradation (Choi et al., 2013). However, recent research has shown that HIPK2 promotes neuronal death in ALS (Lee et al., 2016a). We hypothesized that Wip1 might

be regulated at the protein level by HIPK2 under stress conditions, such as in ALS. To test whether HIPK2 is a negative regulator of Wip1 under mSOD1-induced stress conditions, we determined the effects of either Wip1 or HIPK2 knockdown on the phosphorylation of DNA damage response-signaling proteins in mSOD1 NSC34 cells. The results demonstrated that Wip1 depletion resulted in hyperphosphorylation of ATM, CHK2, and p53 whereas HIPK2 depletion led to Wip1 stabilization and consequent dephosphorylation of its targets such as ATM, CHK2, and p53 (* $p < 0.05$, # $p < 0.05$, and & $p < 0.05$) (Fig. 10A and B). Interaction of HIPK2 with its binding partners was changed after DNA damage (Choi et al., 2008). Therefore, we first determined whether HIPK2 physically interacts with Wip1. Coimmunoprecipitation assays indicated that endogenous Wip1 was associated with HIPK2 both in WT and mSOD1 NSC34 cells, and this interaction was increased in mSOD1 NSC34 cells (Fig. 10C). The polyubiquitination of Wip1 was increased in mSOD1 cells compared with wtSOD cells (Fig. 10D). Next, we determined whether Wip1 is modified by polyubiquitination in a HIPK2-dependent manner. Immunoblot analysis showed that polyubiquitination of Wip1 increased upon co-expression with wild-type HIPK2 in the presence of a proteasome inhibitor MG132 (inhibit proteasome system in order to determine the polyubiquitination level of Wip1) in mSOD1 NSC34 cells (Fig. 10E). We also observed that Flag-Wip1 was polyubiquitinated and that this ubiquitination was inhibited by HIPK2 knockdown (Fig. 10E). Consistent with this observation, polyubiquitination of Wip1 occurred in stressed cells, but was decreased in HIPK2-depleted cells, with the intensity of polyubiquitinated Wip1 gradually increasing following H₂O₂ treatment after 24 h in NSC34 (Fig. 10F). These results suggest that HIPK2 destabilizes Wip1 protein inducing polyubiquitination and proteasome-dependent degradation, and this may be the reason for Wip1 down-regulation in ALS.

Overexpressing Wip1 delayed disease onset, extended lifespan and improved motor performance and inhibited the ATM/CHK2 signaling pathway in ALS mice in SOD1 G93A mice

Three weeks after i.c.v.administration of the Wip1-lentivirus, Transverse sections of the lumbar spinal cord of LV-GFP-Wip1-treated(LV-Wip1 group) mice were stained for anti-MAP2 (a neuronal marker) by immunofluorescence. Wip1(GFP fluorescence) was expressed in MNs (Supplementary Fig. 2A). As shown in Supplementary Fig. 2B-D, LV-Wip1 upregulated Wip1 mRNA and protein levels in the ALS mice compared with LV-GFP control group ($p < 0.01$). To explore whether LV-Wip1 treatment could influence disease onset and progression, we measured the motor function of the ALS mice using the rotarod test. We found that the time to fall was significantly longer in the LV-Wip1-treated ALS mice than in control ALS mice (Supplementary Fig. 3A). The mean time of the onset of motor deficits was found to be 104.6 ± 1.849 days for the LV-GFP group and 117.7 ± 2.205 days for the LV-Wip1 group (Supplementary Fig. 3B, $p < 0.01, n = 15$). Moreover, survival was assessed by Kaplan–Meier survival curves. The results showed that the mean survival time was 136.1 ± 2.824 days for the LV-GFP group and 150.3 ± 2.732 for the LV-Wip1 group (Supplementary Fig. 3C, $p < 0.01, n = 15$). Transverse sections of the lumbar spinal cord were evaluated by counting ChAT-positive cells by immunohistochemical staining in 130d-old ALS mice. Statistical analysis showed a significant reduction in the loss of ChAT-positive neurons in LV-GFP mice compared with LV-Wip1 mice (group means: 7.667 ± 1.453 and 16.33 ± 0.8819 , respectively) (Fig. 3D-G, $P < 0.01, n = 3$). Western blot analysis showed that the levels of pATM and pCHK2 were significantly lower in the LV-Wip1 group mice than in the LV-GFP group mice (Supplementary Fig. 2B, D,

$P < 0.05$). These results indicate that overexpressing Wip1 inhibited the activation of DNA damage response and in ALS mice.

Knocking-down Wip1 accelerated motor deficits, exacerbated the disease process, increased the activity of the ATM/CHK2 signaling pathway in ALS mice

Three weeks after i.c.v. administration of the lentivirus of si-Wip1, we examined Wip1 expression in the lumbar spinal cord. As shown in Supplementary Fig. 4A-C, LV-si-Wip1 downregulated Wip1 mRNA and protein levels in the ALS mice compared with LV-si-NC control group ($p < 0.01$). To explore whether disease onset and progression were influenced in ALS mice after i.c.v. treated LV-siRNA-Wip1 (knocking-down Wip1 in ALS mice), we measured motor function using the rotarod test. We found that the time to fall of ALS mice knocking-down Wip1 was significantly shorter than that in the control mice (Supplementary Fig. 5A). Disease onset also occurred 13 days earlier in ALS mice knocking-down Wip1 compared to the control mice (Supplementary Fig. 5B, 105.1 ± 2.0 versus 91.9 ± 1.9 , respectively; $P < 0.01$, $n = 15$). The median survival (life span) of ALS mice knocking-down Wip1 was 16 days shorter than that of the control mice (Supplementary Fig. 5C, 139.4 ± 3.4 versus 117.1 ± 2.3 respectively, $P < 0.01$, $n = 15$). We performed immunostaining with ChAT in the lumbar spinal cord sections of LV-siRNA-Wip1 and LV-siRNA-NC-treated ALS mice at 130 d age. Quantification of ChAT-positive cells in lumbar spinal cord sections of ALS mice knocking-down Wip1 was less than that in the sections of the control mice (Supplementary Fig. 5D-G < 0.05 , $n = 3$). These results indicate that knocking-down Wip1 accelerated motor deficits and exacerbated the disease process in ALS mice. Western blot analysis showed that levels of pATM and pCHK2 in ALS mice knocking-down Wip1 were significantly higher than those in the control mice (Supplementary Fig. 4A, B, $P < 0.05$, $n = 3$). These results indicate that knocking-down Wip1

upregulated pATM and pCHK2 expression in the ALS mice. Therefore, we conclude that Wip1 knocked-down can promote activation of the DNA damage signaling pathway in ALS mice.

Discussion

Increasing evidence suggests that the DNA damage response plays an important role in the pathology of ALS (Farg et al., 2017; Lopez-Gonzalez et al., 2016). Much remains to be learned regarding how DNA damage response signaling becomes aberrantly elevated in ALS. In this study, we showed an increase in γ -H2AX reactivity (Fig. 4) and cleaved caspase3 immunofluorescent staining (Fig. 5) in hSOD1G93A-positive mice. Wip1 was down-regulated in the hSOD1^{G93A} mouse (Figs. 1 and 2), mSOD1 cell model of ALS (Fig. 3), and chronically stressed NSC34 cells (Fig. 6A; 48 h) but increased in the nucleus of primary neurons from the ALS mouse model (Fig. 3A) and acutely injured NSC34 cells (Fig. 6A; 6 h). Accumulation of Wip1 protein in the nucleus was observed in several cell lines following transient IR-induced DNA damage transcribed by p53 (Fiscella et al., 1997). Several investigators have reported that DNA damage-responsive Wip1 phosphatase is bound to chromatin. Moreover, Wip1 directly dephosphorylates γ -H2AX under genotoxic stress conditions (Macurek et al., 2010). Although the ALS model had greater DNA damage, previous studies have shown that HIPK2 was activated at the end stage in ALS mice (Lee et al., 2016a). In addition, our research indicated that HIPK2 can promote Wip1 degradation through the ubiquitin-proteasome system under the chronic stress condition (Fig. 10). Secondly, another transcription factor, CREB, can regulate Wip1 transcription both basally and after DNA damage independently of p53 (Rossi et al., 2008), which was decreased at the end stage in ALS mice and mSOD1 cells (Rouaux et al., 2003;

Yin et al., 2015). The decrease in both transcription levels and protein stability can cause Wip1 nonresponse to DNA damage. As a result, Wip1 was significantly decreased in the hSOD1^{G93A} mouse (Figs. 1 and 2) and mSOD1 cell model of ALS (Fig. 3). Increased levels of cellular oxidative stress at the early stage of ALS have been reported, such as in primary cultured neurons from SOD^{G93A} fetal mice (Kruman, 1999). However, HIPK2 was not activated (Lee et al., 2016a). Wip1 could respond to the oxidative stress-associated DNA damage. Hence, Wip1 was increased and mainly accumulated in the nucleus in primary neurons from the ALS mouse model (Fig. 3A).

A large number of studies have shown that mutation or deficiency of DNA repair genes in neurons results in the accumulation of DNA damage leading to neuronal dysfunction and neuronal degeneration (Moreira et al., 2001; Poulton et al., 2013; Shen et al., 2010; Takashima et al., 2002; Wang et al., 2013). For example, mutation in FUS(fused in sarcoma), which also participates in DNA repair, leads to the accumulation of DNA strand breaks and neurodegeneration in ALS (Wang et al., 2013). In addition, variants of NEK1, a protein involved in DNA repair, contribute to ALS susceptibility (Kenna et al., 2016). Other studies have reported significantly higher levels of DNA strand breaks in hSOD1^{G93A} transgenic mice (Martin et al., 2007). Moreover, C9ORF72-associated ALS motor neurons exhibit a significant increase in oxidative stress and DNA damage (Lopez-Gonzalez et al., 2016). Collectively, the available data suggest that genome-repair deficiency in conjunction with increased levels of DNA damage are involved in the pathogenesis of ALS and contribute to motor neuron cell death.

The DNA damage response pathway is promptly mobilized by DNA damage to repair the damaged sites by initiating a well-organized signaling network. However, if the DNA damage lesions are beyond repair, the damage-response pathway activates apoptotic signaling cascades to

remove the damaged cells, thus maintaining homeostasis (LeDoux, et al., 2007; Rytter et al., 2007; Weissman et al., 2007;). Recent studies have also indicated that persistent accumulation of DNA damage and inappropriate activation of the DNA damage-responsive ATM signaling pathway may contribute to the pathogenesis of fragile X mental retardation syndrome (fragile X syndrome) and Huntington's disease (Alpatov et al., 2014; Lu et al., 2014; Liu et al., 2012). It is increasingly clear that the DNA damage response is important in neurodegenerative diseases. In the classical model, ATM is activated in response to double-stranded breaks. Activated ATM subsequently phosphorylates and activates Chk2 (Matt and Hofmann, 2016). DNA damage-responsive ATM and its downstream mediator, Chk2, activates p53 (Bode and Dong, 2004). As a consequence, p53 accumulates in the nucleus and promotes apoptotic gene expression, caspase activation, and apoptotic cell death (Prokhorova et al., 2015). The current findings indicated that the DNA damage response was activated in ALS neurons because phosphorylation of ATM and Chk2 was increased in the mSOD1 cells compared to the control cells. Moreover, the expression levels of p53 were higher in the mSOD1 cells compared with the controls (Fig. 5A).

Wip1 is activated by p38 MAPK and p53 in response to various stresses, including UV and g-radiation (Chew et al., 2009; Fiscella et al., 1997; Lowe et al., 2010; Takekawa et al., 2000). Many studies have reported that the up-regulation of Wip1 is associated with tumorigenesis, whereas loss of its function enhances apoptosis in response to DNA damage (Ali et al., 2012; Goloudina et al., 2012; Xia et al., 2009; Yoda et al., 2008). Until now, Wip1 has been characterized as a homeostatic regulator in the DNA damage response, since it dephosphorylates several key proteins, including ATM, ATR, p53, Chk1, Chk2, and H2AX, and restores their expression to normal levels after DNA damage repair (Park et al., 2011). The current results demonstrated that Wip1 knockdown was accompanied by decreased cell viability (Fig. 7C, D,

and E) and further activation of DNA damage response signaling (Fig. 7A and B). In contrast, Flag-Wip1 overexpression in NSC34 cells delayed the activation of DNA damage response signaling (Fig. 8A and B) and inhibited H₂O₂-induced apoptosis (Fig. 8C, E, and F). Moreover, overexpression of exogenous Wip1 blocked aberrant activation of the ATM/CHK2/p53 pathways and improved cell viability in mSOD1 cells (Fig. 9). These data suggest that deregulated expression of Wip1 induces sustainable activation of DNA damage response signaling, which results in the accumulation of proapoptotic genes in vitro model of ALS. In ALS mice, we found that over-expressing Wip1 down-regulated the levels of pATM, pCHK2 in the lumbar spinal cord of ALS mice (Supplementary Fig 2). In addition, we found that over-expression of Wip1 in the central nervous system (CNS) can be delayed the onset of disease symptoms, extended the survival, decreased MN loss improved motor function of SOD1 G93A mice (Supplementary Fig 3). We also confirmed that knocking-down Wip1 increased the levels of pATM and pCHK2 in the lumbar spinal cord of ALS mice (Supplementary Fig 4) and accelerated motor deficits, exacerbated the disease process in ALS mice (Supplementary Fig 5) and. Taken together, these data indicate that Wip1 mediated suppression of ATM/CHK2 activation is a novel molecular mechanism underlying MN death in ALS.

Protein levels of Wip1 are not only regulated by transcription levels but also by post-transcriptional levels under genotoxic conditions (Chew et al., 2009; Choi et al., 2013; Fiscella et al., 1997; Lowe et al., 2010; Takekawa et al., 2000). In unstressed cells, Wip1 is maintained at a low level. Upon transient genotoxic damage, Wip1 can be transcribed to terminate DNA damage response signaling and allow cells to return to normal conditions (Choi et al., 2013). Contrary to significant up-regulation of Wip1 expression in transient DNA damage, the mechanism of persistent DNA damage caused by down-regulation of Wip1 has also been documented

(Crescenzi et al., 2013; Shi et al., 2014; Ugalde et al., 2011). We showed that in the absence of HIPK2, Wip1 levels were elevated in mSOD1-transfected NSC34 cells (Fig. 10A and B) and the interaction between Wip1 and HIPK2 was increased in mSOD1 NSC34 cells (Fig. 10C). We also observed that Flag-Wip1 was polyubiquitinated and that this ubiquitination was inhibited by HIPK2 knockdown, in contrast with polyubiquitination of Wip1 which increased upon co-expression with wild-type HIPK2 in the presence of MG132 (proteasome inhibitor) (Fig. 10E). These results indicated that Wip1 might be regulated by HIPK2 under chronic stress conditions. HIPK2 was initially identified as a corepressor for NK family homeoproteins. Subsequently, HIPK2 was found to participate in various cellular processes such as apoptosis, cell proliferation, and the DNA damage response (Calzado et al., 2007; Choi et al., 2008; Kim et al., 2009; Pierantoni et al., 2007). Evidence suggests that knockout of HIPK2 attenuates neurodegeneration and prolongs survival in the SOD1G93A mouse model (Lee et al., 2016a). Here, we showed that HIPK2 destabilized Wip1 through the ubiquitin protease system in ALS.

In conclusion, the current findings suggest that reduced Wip1 expression combined with DNA damage response activation leads to apoptotic cell death in ALS motor neurons. Wip1 inhibits the ATM-Chk2-p53 pathways, and importantly, it further improves cell viability. Wip1 protects cells from mutant SOD1-induced cell injury. In addition, we showed that HIPK2 promotes Wip1 degradation via the ubiquitin-proteasome system during chronic stress conditions. Collectively, our work supports the hypothesis that deregulated expression of Wip1 induces sustainable activation of DNA damage response signaling, resulting in the accumulation of proapoptotic genes. An image of the proposed mechanism of Wip1 action in DNA damage-induced apoptosis signaling pathways in ALS motor neurons is presented graphical abstract. The other mechanism of activation of DNA damage response by mSOD1 requires further clarification; however, the

results of the present study provide a novel direction for therapeutic options for patients with ALS.

The following are the supplementary data related to this article.

Supplementary Fig. 1 The expression of Wip1 was decreased in the cerebral cortex in a mouse model of amyotrophic lateral sclerosis (ALS). Paraffin sections of cerebral cortex from 130-day-old hSOD1G93A-positive and hSOD1G93A-negative mice were subjected to immunohistochemistry. (A) Wip1 immunoreaction was detected in the cerebral cortex of hSOD1G93A-positive and hSOD1G93A-negative mice. The staining intensity was weaker in hSOD1G93A-positive mice than in hSOD1G93A-negative mice. Scale bar = 20 μ m. The mean intensities of Wip1 were analyzed using Image-Pro Plus 6.0 (n=3/group, 6 sections per mouse). ***p < 0.001. hSOD1G93A -positive and negative mice were euthanized at 130 days post-delivery. (B, C) The results of western blot analysis indicated that the Wip1 protein expression levels were significantly reduced in the cerebral cortex in hSOD1G93A-positive mice. The results were normalized to β -actin and expressed relative to the control (n = 3/group). **p < 0.01. (D) qRT-PCR analysis for relative Wip1 mRNA levels was conducted with samples prepared from cerebral cortex of hSOD1G93A-positive and hSOD1G93A-negative mice. The relative mRNA levels were reduced in hSOD1G93A -positive mice (n = 5). *p < 0.05. Student's t-test.

Supplementary Fig. 2 Enforcement of Wip1 in CNS using lentiviral encoding Wip1 inhibited the ATM/CHK2 signaling pathway in ALS mice. (A) Representative fluorescent images labeled with anti-green fluorescent protein (GFP) in the motor neurons of transgenic mice (red:MAP2; green:GFP-Wip1; blue:DAPI). Scale bar=50 μ m. (B and C) Western blotting and Quantification of Wip1, pATM, ATM, pCHK2, CHK2 protein levels in LV-Wip1 and LV-GFP group

(n=3/group). Wip1 expression in LV-Wip1 group increased significantly compared to the LV-GFP group. pATM and pCHK2 in the LV-Wip1-treated ALS mice were significantly lower than those in the LV-GFP-treated ALS mice. (n=3/group). (D). RT-PCR result analysis. Wip1 mRNA in LV-Wip1 group increased significantly when compared to LV-GFP group (n=5/group), *P<0.05, **P<0.01 vs LV-GFP. Student's t-test.

Supplementary Fig. 3 Overexpressing Wip1 at 90 d of age delays motor deficits in ALS mice. Plots showing the motor function (A) onset of symptoms (B) and the survival time (C) of ALS mice that were i.c.v treated with LV-Wip1/LV-GFP at 90d of age (n=15/group). (D-F) Representative immunohistochemical staining of ChAT in lumbar spinal cord sections of 130-day-old mice in the wild-type littermates, LV-GFP-treated hSOD1G93A mice and LV-Wip1-treated hSOD1G93A mice (n=3/group). (G) The number of MNs in the anterior horns of the spinal cord was counted (n = 3/group, 6 sections per mouse). Statistical analyses of the survival time and the onset time were performed using the Kaplan-Meier survival analysis. Motor function was evaluated with t tests, and the numbers of MNs were analyzed using a one-way ANOVA followed by Tukey's post hoc analysis. Data were compared with those of the LV-GFP group and recorded as the mean \pm SEM. Scale bars: 100 μ m. *p <0.05, **p <0.01.

Supplementary Fig. 4 Knocking-down Wip1 upregulated ATM/CHK2 signaling pathway in ALS mice (A) Western blot showing the protein levels of Wip1, pATM, ATM, pCHK2 and CHK2. Wip1 expression in LV-si-Wip1 group decreased significantly compared to LV-si-NC group (n=3/group). (B) Quantification showed that the pATM and pCHK2 levels in ALS mice knocking-down Wip1 were significantly higher than those in the control mice. (C). RT-PCR result analysis. Wip1 mRNA in LV-si-Wip1 group decreased significantly compared to LV-si-NC group (n=5/group), *P <0.05, **P <0.01, vs LV-si-NC group. Student's t-test.

Supplementary Fig. 5 Delivery of LV-si-Wip1 caused early behavioral changes. (A) Plots showing the rotarod performance of ALS mice knocking-down Wip1 compared to the control mice. (B, C) Onset occurred earlier, and survival was shorter in ALS mice knocking-down Wip1 compared to the control mice. (n=15/group) (D-F) Representative immunohistochemical staining of ChAT in lumbar spinal cord sections of 130-day-old mice in the wild-type littermates, LV-si-Wip1-treated hSOD1G93A mice and LV-si-NC-treated hSOD1G93A mice (n = 3/group, 6 sections per mouse). (G) Quantification of MN loss was more in ALS mice knocking down Wip1 than the LV-si-NC group. Statistical analyses of the survival time and the onset time were performed using the Kaplan-Meier survival analysis. Motor function was evaluated with t tests, and the numbers of MNs were analyzed using a one-way ANOVA followed by Tukey's post hoc analysis. Data were compared with those of the LV-si-NC group and recorded as the mean \pm SEM. Scale bars: 100 μ m. *p < 0.05, **p < 0.01.

Acknowledgments

The authors would like to thank Professor Li-Yu of the Division of Foot-and-mouth Disease, National Key Laboratory of Veterinary Biotechnology, Harbin Veterinary Research Institute, Chinese Academy of Agricultural Sciences for assistance and guidance in experimental techniques. The authors gratefully acknowledge Dr. Neil Cashman from the University of British Columbia, Canada for providing the NSC34 cells.

Funding

This work was supported by the Natural Science Foundation of China [grant number 81571227] and the Major Program of Natural Science Foundation of Heilongjiang Province of China [grant

number ZD201417]. The funding agencies had no role in the study design, the collection, analysis, or interpretation of data, the writing of the report, or the decision to submit the article for publication.

Declaration of interest

None.

Author Contributions

YY and HF designed the study. YY and SW performed the immunohistological experiments. XW and TW performed the immunofluorescence cytochemistry analysis. CZ and WL performed the cell viability assessment. YY and XY performed the immunoblotting and immunoprecipitation experiments. HJ performed cell culture and cell transfection. YW performed the qRT-PCR. HF provided critical commentary on the data analyses, presentation, and the manuscript. HF supervised the experiments and reviewed the article. All authors have approved the final version for publication.

Data Availability Statement

All datasets generated and analyzed for this study are included in the manuscript.

References

Aguirre, N., Beal, M.F., Matson, W.R., and Bogdanov, M.B. (2005). Increased oxidative damage to DNA in an animal model of amyotrophic lateral sclerosis. *Free Radic. Res.* 39, 383-388.

Ali, A.Y., Abedini, M.R., and Tsang, B.K. (2012). The oncogenic phosphatase PPM1D confers cisplatin resistance in ovarian carcinoma cells by attenuating checkpoint kinase 1 and p53 activation. *Oncogene* 31, 2175-2186.

Alpatov, R., Lesch, B.J., Nakamoto-Kinoshita, M., Blanco, A., Chen, S., Stutzer, A., et al. (2014). A chromatin-dependent role of the fragile X mental retardation protein FMRP in the DNA damage response. *Cell* 157, 869-881.

Amante, D.J., Kim, J., Carreiro, S.T., Cooper, A.C., Jones, S.W., Li, T., et al. (2010). Uridine ameliorates the pathological phenotype in transgenic G93A-ALS mice. *Amyotroph. Lateral Scler.* 11, 520-530.

Blasco, H., Garcon, G., Patin, F., Veyrat-Durebex, C., Boyer, J., Devos, D., et al., (2017). Panel of oxidative stress and inflammatory biomarkers in ALS: a pilot study. *Can. J. Neurol. Sci.* 44, 90-95.

Bode, A.M., and Dong, Z. (2004). Post-translational modification of p53 in tumorigenesis. *Nat Rev. Cancer* 4, 793-805.

Bogdanov, M., Brown Jr, R.H., Matson, W., Smart, R., Hayden, D., O'Donnell, H., et al. (2000). Increased oxidative damage to DNA in ALS patients. *Free Radic. Biol. Med.* 29, 652-658.

Boillée, S., Yamanaka, K., Lobsiger, C.S., Copeland, N.G., Jenkins, N.A., Kassiotis, G., et al. (2006). Onset and progression in inherited ALS determined by motor neurons and microglia. *Science* 312: 1389-1392.

Burton MD, Sparkman NL, Johnson RW (2011). Inhibition of interleukin-6 trans-signaling in the brain facilitates recovery from lipopolysaccharide-induced sickness behavior. *J Neuroinflammation*, 8: 54.

Calzado, M.A., Renner, F., Roscic, A., and Schmitz, M.L. (2007). HIPK2: a versatile switchboard regulating the transcription machinery and cell death. *Cell Cycle* 6, 139-143.

Chew, J., Biswas, S., Shreeram, S., Humaidi, M., Wong, E.T., Dhillon, M.K., et al. (2009). WIP1 phosphatase is a negative regulator of NF-kappaB signalling. *Nat. Cell Biol.* 11, 659-666.

Choi, D.W., Na, W., Kabir, M.H., Yi, E., Kwon, S., Yeom, J., et al. (2013). WIP1, a homeostatic regulator of the DNA damage response, is targeted by HIPK2 for phosphorylation and degradation. *Mol. Cell.* 51, 374-385.

Choi, D.W., Seo, Y.M., Kim, E.A., Sung, K.S., Ahn, J.W., Park, S.J., et al. (2008). Ubiquitination and degradation of homeodomain-interacting protein kinase 2 by WD40 repeat/SOCS box protein WSB-1. *J. Biol. Chem.* 283, 4682-4689.

Ciccia, A., and Elledge, S.J. (2010). The DNA damage response: making it safe to play with knives. *Mol. Cell.* 40, 179-204.

Crescenzi, E., Raia, Z., Pacifico, F., Mellone, S., Moscato, F., Palumbo, G., et al. (2013). Down-regulation of wild-type p53-induced phosphatase 1 (Wip1) plays a critical role in regulating several p53-dependent functions in premature senescent tumor cells. *J. Biol. Chem.* 288, 16212-16224.

DeJesus-Hernandez, M., Mackenzie, I.R., Boeve, B.F., Boxer, A.L., Baker, M., Rutherford, N.J., et al. (2011). Expanded GGGGCC hexanucleotide repeat in noncoding region of C9ORF72 causes chromosome 9p-linked FTD and ALS. *Neuron* 72, 245-256.

Ditch, S., and Paull, T.T. (2012). The ATM protein kinase and cellular redox signaling: beyond the DNA damage response. *Trends Biochem. Sci.* 37, 15-22.

Doré, S., Takahashi, M., Ferris, C.D., Hester, L.D., Guastella, D., and Snyder, S.H. (1999). Bilirubin, formed by activation of heme oxygenase-2, protects neurons against oxidative stress injury. *Proc. Natl. Acad. Sci. U. S. A.* 96, 2445-2450.

Farg, M.A., Konopka, A., Soo, K.Y., Ito, D., and Atkin, J.D. (2017). The DNA damage response (DDR) is induced by the C9orf72 repeat expansion in amyotrophic lateral sclerosis. *Hum. Mol. Genet.* 26, 2882-2896.

Feng, H.L., Leng, Y., Ma, C.H., Zhang, J., Ren, M., and Chuang, D.M. (2008). Combined lithium and valproate treatment delays disease onset, reduces neurological deficits and prolongs survival in an amyotrophic lateral sclerosis mouse model. *Neuroscience*, 155, 567-572.

Ferrante, R.J., Browne, S.E., Shinobu, L.A., Bowling, A.C., Baik, M.J., MacGarvey, U., et al. (1997). Evidence of increased oxidative damage in both sporadic and familial amyotrophic lateral sclerosis. *J. Neurochem.* 69: 2064-2074.

Fiscella, M., Zhang, H., Fan, S., Sakaguchi, K., Shen, S., Mercer, W.E., et al. (1997). Wip1, a novel human protein phosphatase that is induced in response to ionizing radiation in a p53-dependent manner. *Proc. Natl. Acad. Sci. U. S. A.* 94, 6048-6053.

Gao, R., Liu, Y., Silva-Fernandes, A., Fang, X., Paulucci-Holthauzen, A., Chatterjee, A., et al. (2015). Inactivation of PNKP by mutant ATXN3 triggers apoptosis by activating the DNA damage-response pathway in SCA3. *PLoS Genet.* 11, e1004834.

Goloudina, A.R., Tanoue, K., Hammann, A., Fourmaux, E., Le Guezennec, X., Bulavin, D.V., et al. (2012). Wip1 promotes RUNX2-dependent apoptosis in p53-negative tumors and protects normal tissues during treatment with anticancer agents. *Proc. Natl. Acad. Sci. U. S. A.* 109: E68-75.

Gurney, M.E., Pu, H., Chiu, A.Y., Dal Canto, M.C., Polchow, C.Y., Alexander, D.D., et al. (1994). Motor neuron degeneration in mice that express a human Cu, Zn superoxide dismutase mutation. *Science* 264, 1772-1775.

Kenna, K.P., van Doormaal, P.T., Dekker, A.M., Ticozzi, N., Kenna, B.J., Diekstra, F.P., et al. (2016). NEK1 variants confer susceptibility to amyotrophic lateral sclerosis. *Nat. Genet.* 48, 1037-1042.

Kiernan, M.C., Vucic, S., Cheah, B.C., Turner, M.R., Eisen, A., Hardiman, O., et al. (2011). Amyotrophic lateral sclerosis. *Lancet* 377, 942-955.

Kim, S.Y., Choi, D.W., Kim, E.A., and Choi, C.Y. (2009). Stabilization of HIPK2 by escape from proteasomal degradation mediated by the E3 ubiquitin ligase Siah1. *Cancer Lett.* 279, 177-184.

Kruman, I.I., Pedersen, W.A., Springer, J.E., and Mattson, M.P. (1999). ALS-linked Cu/Zn-SOD mutation increases vulnerability of motor neurons to excitotoxicity by a mechanism involving increased oxidative stress and perturbed calcium homeostasis. *Exp. Neurol.* 160, 28-39.

LeDoux, S.P., Druzhyna, N.M., Hollensworth, S.B., Harrison, J.F., and Wilson, G.L. (2007). Mitochondrial DNA repair: a critical player in the response of cells of the CNS to genotoxic insults. *Neuroscience* 145, 1249-1259.

Lee, S., Shang, Y., Redmond, S.A., Urisman, A., Tang, A.A., Li, K.H., et al. (2016a). Activation of HIPK2 promotes ER stress-mediated neurodegeneration in amyotrophic lateral sclerosis. *Neuron* 91, 41-55.

Lee, S.H., Choi, N.Y., Yu, H.J., Park, J., Choi, H., Lee, K.Y., et al. (2016b). Atorvastatin protects NSC-34 motor neurons against oxidative stress by activating PI3K, ERK and free radical scavenging. *Mol. Neurobiol.* 53, 695-705.

Liu, W., Jiang, F., Bi, X., and Zhang, Y.Q. (2012). *Drosophila* FMRP participates in the DNA damage response by regulating G2/M cell cycle checkpoint and apoptosis. *Hum. Mol. Genet.* 21, 4655-4668.

Li M, Ona VO, Guegan C, Chen M, Jackson-Lewis V, Andrews LJ, Olszewski AJ, Stieg PE, Lee JP, Przedborski S, Friedlander RM (2000) Functional role of caspase-1 and caspase-3 in an ALS transgenic mouse model. *Science* 288:335–339.

Lopez-Gonzalez, R., Lu, Y., Gendron, T.F., Karydas, A., Tran, H., Yang, D., et al. (2016). Poly(GR) in C9ORF72-Related ALS/FTD compromises mitochondrial function and increases oxidative stress and DNA damage in iPSC-derived motor neurons. *Neuron* 92, 383-391.

Lowe, J.M., Cha, H., Yang, Q., and Fornace, A.J., Jr. (2010). Nuclear factor-kappaB (NF-kappaB) is a novel positive transcriptional regulator of the oncogenic Wip1 phosphatase. *J. Biol. Chem.* 285, 5249-5257.

Lu, X.H., Mattis, V.B., Wang, N., Al-Ramahi, I., van den Berg, N., Fratantoni, S.A., et al. (2014). Targeting ATM ameliorates mutant Huntingtin toxicity in cell and animal models of Huntington's disease. *Sci. Transl. Med.* 6, 268ra178.

Ludolph AC, Bendotti C, Blaugrund E, Hengerer B, Loffler JP, Martin J., et al. (2007) Guidelines for the preclinical in vivo evaluation of pharmacological active drugs for ALS/MND:report on the 142nd ENMC international workshop. *Amyotroph Lateral Scler* 8:217–223.

Ma, X., Han, J., Wu, Q., Liu, H., Shi, S., Wang, C., et al. (2015). Involvement of dysregulated Wip1 in manganese-induced p53 signaling and neuronal apoptosis. *Toxicol. Lett.* 235, 17-27.

Macurek, L., Lindqvist, A., Voets, O., Kool, J., Vos, H.R., and Medema, R.H. (2010). Wip1 phosphatase is associated with chromatin and dephosphorylates gammaH2AX to promote checkpoint inhibition. *Oncogene* 29, 2281-2291.

Madabhushi, R., Pan, L., and Tsai, L.H. (2014). DNA damage and its links to neurodegeneration. *Neuron* 83, 266-282.

Maier, O., Bohm, J., Dahm, M., Bruck, S., Beyer, C., and Johann, S. (2013). Differentiated NSC-34 motoneuron-like cells as experimental model for cholinergic neurodegeneration. *Neurochem. Int.* 62, 1029-1038.

Majoor-Krakauer, D., Willems, P.J., and Hofman, A. (2003). Genetic epidemiology of amyotrophic lateral sclerosis. *Clin. Genet.* 63, 83-101.

Martin, L.J. (2007). Transgenic mice with human mutant genes causing Parkinson's disease and amyotrophic lateral sclerosis provide common insight into mechanisms of motor neuron selective vulnerability to degeneration. *Rev. Neurosci.* 18,115-136.

Martin, L.J., Liu, Z., Chen, K., Price, A.C., Pan, Y., Swaby, J.A., and Golden, W.C. (2007). Motor neuron degeneration in amyotrophic lateral sclerosis mutant superoxide dismutase-1 transgenic mice: mechanisms of mitochondriopathy and cell death. *J. Comp. Neurol.* 500, 20-46.

Matt, S., and Hofmann, T.G. (2016). The DNA damage-induced cell death response: a roadmap to kill cancer cells. *Cell. Mol. Life Sci.* 73, 2829-2850. doi: 10.1007/s00018-016-2130-4

McKinnon, P.J. (2004). ATM and ataxia telangiectasia. *EMBO Rep.* 5, 772-776.

Mitsumoto, H., Santella, R.M., Liu, X., Bogdanov, M., Zipprich, J., Wu, H.C., et al. (2008). Oxidative stress biomarkers in sporadic ALS. *Amyotroph. Lateral Scler.* 9, 177-183.

Moreira, M.C., Barbot, C., Tachi, N., Kozuka, N., Uchida, E., Gibson, T., et al. (2001). The gene mutated in ataxia-ocular apraxia 1 encodes the new HIT/Zn-finger protein aprataxin. *Nat. Genet.* 29,189-193.

Murata, T., Ohtsuka, C., and Terayama, Y. (2008). Increased mitochondrial oxidative damage and oxidative DNA damage contributes to the neurodegenerative process in sporadic amyotrophic lateral sclerosis. *Free Radic. Res.* 42, 221-225.

Park, H.K., Panneerselvam, J., Dudimah, F.D., Dong, G., Sebastian, S., Zhang, J., et al. (2011). Wip1 contributes to cell homeostasis maintained by the steady-state level of Wtp53. *Cell Cycle* 10, 2574-2582.

Pierantoni, G.M., Rinaldo, C., Mottotese, M., Di Benedetto, A., Esposito, F., Soddu, S., et al. (2007). High-mobility group A1 inhibits p53 by cytoplasmic relocalization of its proapoptotic activator HIPK2. *J. Clin. Invest.* 117, 693-702.

Poulton, C., Oegema, R., Heijnsman, D., Hoozeboom, J., Schot, R., Stroink, H., et al. (2013). Progressive cerebellar atrophy and polyneuropathy: expanding the spectrum of PNKP mutations. *Neurogenetics* 14, 43-51.

Prokhorova, E.A., Zamaraev, A.V., Kopeina, G.S., Zhivotovsky, B., and Lavrik, I.N. (2015). Role of the nucleus in apoptosis: signaling and execution. *Cell. Mol. Life Sci.* 72, 4593-4612.

Robberecht, W., and Philips, T. (2013). The changing scene of amyotrophic lateral sclerosis. *Nat. Rev. Neurosci.* 14, 248-264.

Rosen, D.R., Siddique, T., Patterson, D., Figlewicz, D.A., Sapp, P., Hentati, A., et al. (1993). Mutations in Cu/Zn superoxide dismutase gene are associated with familial amyotrophic lateral sclerosis. *Nature* 364, 362.

Rossi, M., Demidov, O.N., Anderson, C.W., Appella, E., and Mazur, S.J. (2008). Induction of PPM1D following DNA-damaging treatments through a conserved p53 response element coincides with a shift in the use of transcription initiation sites. *Nucleic Acids Res.* 36, 7168-7180.

Rothstein, J.D. (2009). Current hypotheses for the underlying biology of amyotrophic lateral sclerosis. *Ann. Neurol.* 65 Suppl 1, S3-9.

Rouaux, C., Jokic, N., Mbebi, C., Boutillier, S., Loeffler, J.P., and Boutillier, A.L. (2003). Critical loss of CBP/p300 histone acetylase activity by caspase-6 during neurodegeneration. *EMBO J.* 22, 6537-6549.

Ryter, S.W., Kim, H.P., Hoetzel, A., Park, J.W., Nakahira, K., Wang, X., and Choi, A.M. (2007). Mechanisms of cell death in oxidative stress. *Antioxid. Redox Signal* 9, 49-89.

Saccon, R.A., Bunton-Stasyshyn, R.K., Fisher, E.M., and Fratta, P. (2013). Is SOD1 loss of function involved in amyotrophic lateral sclerosis? *Brain* 136(Pt 8), 2342-2358.

Shen, J., Gilmore, E.C., Marshall, C.A., Haddadin, M., Reynolds, J.J., Eyaid, W., et al. (2010). Mutations in PNKP cause microcephaly, seizures and defects in DNA repair. *Nat. Genet.* 42, 245-249.

Shi, Y., Nikulenkov, F., Zawacka-Pankau, J., Li, H., Gabdoulline, R., Xu, J., et al. (2014). ROS-dependent activation of JNK converts p53 into an efficient inhibitor of oncogenes leading to robust apoptosis. *Cell Death Differ.* 21, 612-623.

Shibata, N., Nagai, R., Miyata, S., Jono, T., Horiuchi, S., Hirano, A., et al. (2000). Nonoxidative protein glycation is implicated in familial amyotrophic lateral sclerosis with superoxide dismutase-1 mutation. *Acta Neuropathol.* 100, 275-284.

Shiloh, Y., and Ziv, Y. (2013). The ATM protein kinase: regulating the cellular response to genotoxic stress, and more. *Nat. Rev. Mol. Cell. Biol.* 14, 197-210.

Shreeram, S., Demidov, O.N., Hee, W.K., Yamaguchi, H., Onishi, N., Kek, C., et al. (2006a). Wip1 phosphatase modulates ATM-dependent signaling pathways. *Mol. Cell.* 23, 757-764.

Shreeram, S., Hee, W.K., Demidov, O.N., Kek, C., Yamaguchi, H., Fornace, A.J., Jr., et al. (2006b). Regulation of ATM/p53-dependent suppression of myc-induced lymphomas by Wip1 phosphatase. *J. Exp. Med.* 203, 2793-2799.

Singhal, A., Morris, V.B., Labhasetwar, V., and Ghorpade, A. (2013). Nanoparticle-mediated catalase delivery protects human neurons from oxidative stress. *Cell Death Dis.* 4, e903.

Song, J.Y., Ryu, S.H., Cho, Y.M., Kim, Y.S., Lee, B.M., Lee, S.W., and Choi, J. (2013). Wip1 suppresses apoptotic cell death through direct dephosphorylation of BAX in response to gamma-radiation. *Cell Death Dis.* 4, e744.

Sreedharan, J., Blair, I.P., Tripathi, V.B., Hu, X., Vance, C., Rogelj, B., et al. (2008). TDP-43 mutations in familial and sporadic amyotrophic lateral sclerosis. *Science* 319, 1668-1672.

Takashima, H., Boerkoel, C.F., John, J., Saifi, G.M., Salih, M.A., Armstrong, D., et al. (2002). Mutation of TDP1, encoding a topoisomerase I-dependent DNA damage repair enzyme, in spinocerebellar ataxia with axonal neuropathy. *Nat. Genet.* 32, 267-272.

Takekawa, M., Adachi, M., Nakahata, A., Nakayama, I., Itoh, F., Tsukuda, H., et al. (2000). p53-inducible wip1 phosphatase mediates a negative feedback regulation of p38 MAPK-p53 signaling in response to UV radiation. *EMBO J.* 19, 6517-6526.

Turner, B.J., and Talbot, K. (2008). Transgenics, toxicity and therapeutics in rodent models of mutant SOD1-mediated familial ALS. *Prog. Neurobiol.* 85, 94-134.

- Turner, M.R., Grosskreutz, J., Kassubek, J., Abrahams, S., Agosta, F., Benatar, M., et al. (2011). Towards a neuroimaging biomarker for amyotrophic lateral sclerosis. *Lancet Neurol.* 10, 400-403. doi: 10.1016/S1474-4422(11)70049-7
- Ugalde, A.P., Ramsay, A.J., de la Rosa, J., Varela, I., Mariño, G., Cadiñanos, J., et al. (2011). Aging and chronic DNA damage response activate a regulatory pathway involving miR-29 and p53. *EMBO J.* 30, 2219-2232.
- Wang, S.Y., Ren, M., Jiang, H.Z., Wang, J., Jiang, H.Q., Yin, X., et al. (2015). Notch pathway is activated in cell culture and mouse models of mutant SOD1-related familial amyotrophic lateral sclerosis, with suppression of its activation as an additional mechanism of neuroprotection for lithium and valproate. *Neuroscience* 301, 276-288.
- Wang, W.Y., Pan, L., Su, S.C., Quinn, E.J., Sasaki, M., Jimenez, J.C., et al. (2013). Interaction of FUS and HDAC1 regulates DNA damage response and repair in neurons. *Nat. Neurosci.* 16, 1383-1391.
- Weissman, L., de Souza-Pinto, N.C., Stevnsner, T., and Bohr, V.A. (2007). DNA repair, mitochondria, and neurodegeneration. *Neuroscience* 145, 1318-1329.
- Xia, Y., Ongusaha, P., Lee, S.W., and Liou, Y.C. (2009). Loss of Wip1 sensitizes cells to stress- and DNA damage-induced apoptosis. *J. Biol. Chem.* 284, 17428-17437.
- Yin, X., Ren, M., Jiang, H., Cui, S., Wang, S., Jiang, H., et al. (2015). Down-regulated AEG-1 together with inhibited PI3K/Akt pathway is associated with reduced viability of motor neurons in an ALS model. *Mol. Cell. Neurosci.* 68, 303-313.

Yoda, A., Toyoshima, K., Watanabe, Y., Onishi, N., Hazaka, Y., Tsukuda, Y., et al. (2008). Arsenic trioxide augments Chk2/p53-mediated apoptosis by inhibiting oncogenic Wip1 phosphatase. *J. Biol. Chem.* 283, 18969-18979.

Figure 1. Wip1 expression was decreased in motor neurons in a mouse model of amyotrophic lateral sclerosis (ALS). Paraffin sections of spinal cords from 130-day-old hSOD1^{G93A}-positive and hSOD1^{G93A}-negative mice were subjected to immunohistochemistry. (A) Wip1 immunoreaction was detected in the anterior horn neurons (black arrow) of the spinal cord from both hSOD1^{G93A}-positive and hSOD1^{G93A}-negative mice. The staining intensity was weaker in hSOD1^{G93A}-positive mice than in hSOD1^{G93A}-negative mice. Scale bar = 50 μ m. (B) The mean intensities of Wip1 were analyzed using Image-Pro Plus 6.0 (n = 3/group, 6 sections per mouse). **p < 0.01. hSOD1^{G93A}-positive and negative mice were euthanized at 130 days post-delivery. (C, D) The results of western blot analysis indicated that the Wip1 protein levels were significantly reduced in hSOD1^{G93A}-positive mice. The results were normalized to β -actin and expressed relative to the control (n = 3). *p < 0.05. (E) qRT-PCR analysis for relative Wip1 mRNA levels was conducted with samples prepared from hSOD1^{G93A}-positive and hSOD1^{G93A}-negative mice. The relative mRNA levels were reduced in hSOD1^{G93A}-positive mice (n = 5). *p < 0.05.

Figure 2. The intensity of Wip1 immunofluorescence staining was decreased in spinal cord anterior horn neurons in a mouse model of amyotrophic lateral sclerosis (ALS). Paraffin sections of spinal cords from 130-day-old hSOD1^{G93A}-positive and hSOD1^{G93A}-negative mice were subjected to double immunofluorescence staining with anti-Wip1 and MAP-2 antibodies,

followed by the respective fluorescence-conjugated secondary antibodies. 4,6-Diamidino-2-phenylindole (DAPI) was used to label the cell nucleus (blue). Wip1 expression (green) was identified in neurons (red). (n = 3/group, 6 sections per mouse). Scale bar = 20 μ m.

Figure 3. Expression of Wip1 was increased in primary cultured mSOD1-positive neurons, but decreased in mSOD1 stably transfected NSC34 cells. (A) Primary neurons were prepared from the brain cortex of E16–18 fetal mice. The genotype was determined by polymerase chain reaction (PCR). The cells were fixed and subjected to immunofluorescence staining with anti-Wip1 (green) antibody. 4,6-Diamidino-2-phenylindole (DAPI) (blue) was used for nuclear staining. Scale bar = 25 μ m. (B) qRT-PCR analysis showed that relative Wip1 mRNA levels of mSOD1-positive neurons and mSOD1-negative neurons (n = 5). **p < 0.01. (C) NSC34 cells were cultured, then transfected with empty puromycin lentivirus vector (pLV cells), a lentiviral vector containing wild-type human SOD1 (wtSOD1 cells), or human SOD1 mutant G93A (mSOD1 cells). mRNA levels of Wip1 in NSC34, pLV, wtSOD1, and mSOD1 cells were determined using quantitative real-time PCR (n = 5). *p < 0.05 (D and E). Western blot analysis was performed to determine the levels of Wip1 from NSC34 cells and pLV, wtSOD1, and mSOD1 stably transfected cells (n = 3). *p < 0.05.

Figure 4. Immunofluorescence staining for γ -H2AX in hSOD1^{G93A}-positive and negative mice. An increase in γ -H2AX reactivity (green) was identified in hSOD1^{G93A}-positive mice. (n = 3/group, 6 sections per mouse). Scale bar = 25 μ m.

Figure 5. Immunofluorescence staining for cleaved caspase3 in hSOD1^{G93A}-positive and negative mice. An increase in cleaved caspase3 immunofluorescent staining (green) was identified in hSOD1^{G93A}-positive mice. (n = 3/group, 6 sections per mouse). Scale bar = 25 μ m.

Figure 6. Down-regulation of Wip1 is required for DNA damage response activation during H₂O₂-induced DNA damage. (A) NSC34 cells were maintained without serum for 4 h, followed by 100 μ M H₂O₂ treatment of 3, 6, 24, and 48 h. Immunoblotting was performed with the indicated antibodies. (B) Quantification of the protein levels of Wip1, pATM, pCHK2, p-p53, and cleaved caspase 3 (n = 3). *p < 0.05, **p < 0.01, *** p < 0.001 vs. controls. (C) Primary cultured neurons were treated with 50 μ M H₂O₂ for 1, 6, and 12 h and double immunofluorescence staining was performed. Fixed primary cultured neurons were stained with anti-Wip1 antibody (green) and anti-MAP2 antibody (red). Scale bar = 200 μ m.

Figure 7. Down-regulation of Wip1 promotes DNA damage response activation and neuronal cell death in NSC34 cells. (A) NSC34 cells were transfected with si-Wip1 RNA or si-NC RNA sequences for 24 h and then exposed to H₂O₂ (100 μ M) for the indicated time, followed by immunoblotting of the indicated antibody. (B) Quantitative analysis of the protein levels in DNA damage response signaling after Wip1 knockdown (n = 3) (*p < 0.05, **p < 0.01, ***p < 0.001). (C and D) Annexin-V/PI apoptotic analysis of the effect of Wip1 knockdown on H₂O₂-induced cell death of NSC34 cells (n = 3) (*p < 0.05). (E) Cell viability was quantified using the CCK8 assay. H₂O₂ decreased the viability of NSC34 cells, whereas the effect was exacerbated by Wip1 knockdown (n = 5) (*p < 0.05, **p < 0.01).

Figure 8. Overexpression of Wip1 ameliorated H₂O₂-induced DNA damage response signaling and cytotoxicity in NSC34 cells. (A) NSC34 cells were transfected with Flag or Flag-Wip1 and then exposed to H₂O₂ (100 μ M) for the indicated time, followed by immunoblotting of the indicated antibody. (B) Quantitative analysis of the protein levels in DNA damage response signaling after Wip1 overexpression (n = 3). *p < 0.05, **p < 0.01, ***p < 0.001 (C and D) Annexin-V/PI apoptotic analysis of the effect of Wip1 overexpression on H₂O₂-induced cell

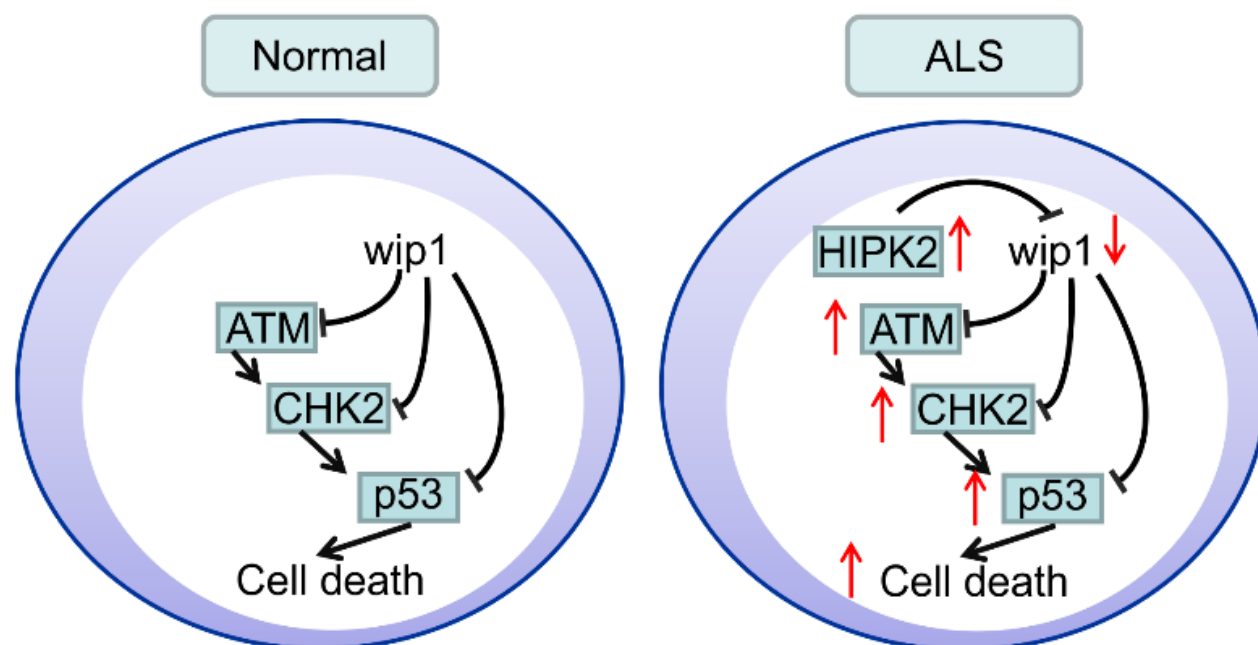
death of NSC34 cells ($n = 3$). $*p < 0.05$, $**p < 0.01$ (E) Cell viability was quantified using the CCK8 assay. H_2O_2 decreased the viability of NSC34 cells, whereas the effect was partially reversed by Wip1 overexpression ($n = 5$). $*p < 0.05$, $**p < 0.01$.

Figure 9. Wip1 confers cytoprotection against mutant SOD1-induced toxicity. (A) Cell lysates from NSC34, pLV, wtSOD1, and mSOD1 cells were collected for immunoblotting with the indicated antibodies. (B) Quantification of relative protein levels of p-ATM, p-Chk2, and p-p53 with β -actin as a loading control ($n = 3$). $***p < 0.001$ (C) wtSOD cells and mSOD1 cells were transiently transfected with Flag-tagged Wip1 using Lipofectamine2000. After 48 h, western blot analysis was performed with the indicated antibodies. (D) Quantitative analysis of the protein levels in the DNA damage response signaling after Wip1 overexpression ($n = 3$). $*p < 0.05$. (E) Cell viability was quantified using the CCK8 assay ($n = 5$). $**p < 0.01$ versus the corresponding empty puromycin lentivirus vector control or SOD1 WT-expressing cells; $###p < 0.001$ versus the corresponding control cells lacking exogenous Wip1.

Figure 10. HIPK2 promotes ubiquitination and degradation of Wip1 in mSOD1 cells. (A) mSOD1 cells were transfected with control siRNA, si-Wip1, or si-HIPK2 and harvested. Cell lysates were analyzed by immunoblotting with indicated antibodies. (B) Quantitative analysis of the protein levels after Wip1 or HIPK2 knockdown ($n = 3$). $*p < 0.05$, $\#p < 0.05$, and $\&p < 0.05$ vs. corresponding controls. (C) wtSOD1 and mSOD1 cells were harvested and lysates were immunoprecipitated with anti-HIPK2 antibody, followed by immunoblotting with the anti-Wip1 antibodies. (D) wtSOD1 cells and mSOD1 cells were transfected with Flag-Wip1. Twenty-four hours later and after incubation with 10 μ M MG132 for 4 h, the supernatants of the cell lysates were immunoprecipitated with mouse monoclonal antibodies against Flag followed by

immunoblotting with anti-ubiquitin (Ub) antibody. (E) mSOD1 NSC34 cells were co-transfected with Flag-Wip1 with HA-HIPK2 expression plasmids or siRNA targeting HIPK2 as indicated for 24 h and treated with MG132 4 h prior to harvest, and the supernatants of the cell lysates were immunoblotted with the indicated antibodies or immunoprecipitated with anti-Flag antibody, followed by immunoblotting with anti-ubiquitin (Ub) antibody. (F) NSC34 cells were transfected with control siRNA or siRNA targeting HIPK2 in combination with the Flag-Wip1 expression plasmid, followed by treatment with MG132. Cells were harvested at the indicated time points after H₂O₂ treatment, and lysates were immunoprecipitated with anti-Flag antibody, followed by immunoblotting with the indicated antibodies.

Graphical Abstract



Graphical Abstract: Figure summarized entire findings of this study in a graphical way.

Schematic representation highlighting the role of Wip1 in the development of amyotrophic lateral sclerosis (ALS). Wip1 directly targets pATM, pCHK2, and p-p53 to regulate DNA damage response activity. Inhibition of Wip1 leads to aberrant activation of DNA damage response signaling, resulting in enhanced cell death. HIPK2 is partial responsible for the down-regulation of Wip1 in ALS.

Highlights

- Wip1 expression was decreased in both in vivo and in vitro models of ALS;
- Wip1 improved mSOD1 cell viability and induced inhibition of the DNA damage response in mSOD1 cells;
- Wip1 can delay the onset of disease symptoms, extended the survival, decreased MN loss improved motor function and inhibit the DNA-damage response in SOD1 G93A mice
- HIPK2 promotes Wip1 degradation through the ubiquitin-proteasome system in mSOD1 cells.